Radiation Measurements 165 (2023) 106951

Contents lists available at ScienceDirect

Radiation Measurements

journal homepage: www.elsevier.com/locate/radmeas

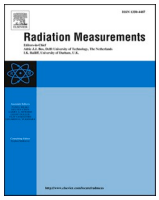

Monte Carlo simulation of a simple and fast method to experimentally determine the partial sensitivity of a bare LR-115 detector using planar alpha sources

Patrizia Pereyra [a,*], Daniel Palacios [a,c], Elisabeth Mateus Yoshimura [b], Laszlo Sajo-Bohus [c]

[a] Departamento de Ciencias, Pontificia Universidad Católica Del Perú, Lima, Peru
[b] Departamento de Física Nuclear, Instituto de Física, Universidade de São Paulo, Brazil
[c] Universidad Simón Bolívar, Caracas, Venezuela

ARTICLE INFO

Keywords:
Monte Carlo Simulation
Partial sensitivity
Bare LR-115 detector
Planar alpha source

ABSTRACT

Partial sensitivity of the bare LR-115 detector (K_B) to radon or thoron, or any of their airborne progeny, is an essential component in the detector's calibration factor. Its experimental determination is complex, requires expensive and sophisticated instruments and facilities, and is time consuming. Using the TRACK_TEST and SRIM programs, and Monte Carlo simulations, the possibility of a simple and fast method to determine K_B experimentally was demonstrated. The method is based on calculations of the average value of detection efficiencies (i.e., the cumulative efficiency) for alpha particles emitted by a planar alpha source placed at different distances from detectors. Source radius can be estimated from the energy of emitted alpha particles, detector radius, and parameters dependent on etching conditions. Varying the emission energy of alpha particles, the source and detector radii, and the source-detector distance step length, an average value of 0.02 tracks. cm^{-2} per Bq.d.m^{-3} (0.22 cm) was obtained assuming standard etching conditions. In addition to alpha electrodeposited sources, sealed sources such as those built with anodized aluminium sheets proved to be suitable for this proposal. Experimentally, K_B can be estimated from: track densities registered in detectors exposed at different distances from the source, range of distances that produce visible tracks, and source activity. The developed method is much simpler and faster than the conventional method that uses standard sources of radon and its progeny and large chamber with controlled conditions.

1. Introduction

For several years the bare LR-115 detector has been used to measure total alpha in air (Baggs and Wong, 1987; Banjanac et al., 2006), PAEC of radon progeny or radon concentration (Loffredo et al., 2022; Kitson-Mills et al., 2019), proxy equilibrium factor (Yu and Nikezic, 2011) and equilibrium factor (Abo-Elmagd et al., 2006; Nader, 2019), and for other applications (Mitev et al., 2020; Pressyanov, 2022). Recent intercomparison results of passive radon detectors demonstrated satisfactory accuracy and precision of the bare LR-115 detector in measurements (Miller and Howarth 2022).

The LR-115 detector kept in bare mode registers alpha tracks related to concentrations of ^{222}Rn, ^{220}Rn and their airborne alpha-emitting progenies. Their responses are expressed by the partial sensitivities K_B to each of these species (i.e., the number of tracks per unit area and time of exposure, per unit activity concentration of that species). Using Monte Carlo simulations, K_B (m^{-2}. s^{-1}. Bq^{-1}. m^3 or just m) for ^{222}Rn, ^{218}Po and ^{214}Po were found to be the same for removed layer smaller than 8 μm (Nikezic and Yu, 2010; Yu et al., 2005; Nikezic and Yu, 2007). Equality of partial sensitivities has been demonstrated theoretically and experimentally (Eappen and Mayya, 2004; Leung et al., 2006). For standard etching conditions the aforementioned authors indicated a value of 0.02 tr. cm^{-2}. Bq.d.m^{-3} (0.23 cm). However, the detector response strongly depends on etching conditions and track reading mode (Stevanovic et al., 2022). Thus, it is not recommended to use the value reported in literature, but rather that each laboratory determine the value corresponding to its etching and reading conditions.

It is important to know K_B because if the equilibrium factor F_e is also

* Corresponding author.
E-mail addresses: ppereyr@pucp.edu.pe (P. Pereyra), dpalaciosf@pucp.edu.pe, palacios@usb.ve (D. Palacios), e.yoshimura@if.usp.br (E.M. Yoshimura), lsajo@usb.ve (L. Sajo-Bohus).

https://doi.org/10.1016/j.radmeas.2023.106951
Received 19 January 2023; Received in revised form 3 May 2023; Accepted 12 May 2023
Available online 13 May 2023

known, then the actual calibration factor of the bare LR-115 detector can be determined as $K_B(1+2F_e)$ (Eappen and Mayya, 2004). Furthermore, using K_B, the track density registered on the bare LR-115, and the radon concentration determined by some passive method, the proxy equilibrium factor F_p can be calculated (Yu et al., 2005; Yu and Nikezic, 2011). Since the relationship between F_p and the equilibrium factor F_e is known, it becomes possible to estimate this last factor which is essential in calculating the inhalation dose.

The experimental determination of partial sensitivities to radon isotopes and their progeny is very difficult since it is not possible to separate them physically and usually they are not in equilibrium. Since K_B cannot be measured directly, its estimation becomes more complex, requiring considerable time and expensive and sophisticated instruments and facilities. The most common method is exposing bare LR-115 detectors in a special chamber to well-known reference concentrations of radon and its progeny. In addition to the equilibrium factor, other parameters are controlled during the exposure period and only a few laboratories worldwide have this type of chamber, e.g., the walk-in exposure chamber at the Health Protection Agency (HPA), Chilton, UK (Miles et al., 1984).

Considering the simplicity and cheapness of the nuclear track methodology for radon measurements, it would be advisable to develop a simpler, cheaper, and faster method for the estimation of K_B, taking advantage of the fact that it is the same for any species. The objective of this study is to demonstrate through simulations the possibility of estimating K_B experimentally through a simpler and faster method, based on the exposure of LR-115 detectors to a planar alpha source. A Monte Carlo simulation code will be developed to evaluate the response of LR-115 detectors placed at different distances from a planar ^{241}Am source. TRACK_TEST program (Nikezic et al., 2021) will be used to perform simulations of etched track profiles in order to obtain the energy window and the dependence of the critical angle with the alpha particle energy. The relationships between residual energy and distance travelled by alpha particles in air will be determined with the help of the SRIM-2013 program (Ziegler, 2013).

2. Theoretical estimates of partial sensitivities

An alpha particle can produce an etched track visible with an optical microscope, if it is emitted from the so-called effective volume. The total number of tracks registered in the detector can be computed by integrating the fluences coming from the various points in the effective volume. Thus, K_B can be expressed in a simplified way as (Eappen and Mayya, 2004):

$$K_B = \frac{1}{4}\int_{\theta_c}^{\pi/2} \sin(2\theta)[R_{\max}(\theta) - R_{\min}(\theta)]d\theta \quad (1)$$

where θ is the incident angle ranging from to the critical angle (θ_c) to normal incidence ($\pi/2$); $R_{\min}$ and $R_{\max}$ are the alpha particle ranges for $E_{\max}$ and $E_{\min}$ of the energy window, respectively. Since the integration should be performed over the entire effective volume, Eq. (1) is equivalent to the sum of partial sensitivities obtained for each horizontal cross-section of the effective volume, divided by the total number of sections in which the effective volume was cut, i.e., K_B is equivalent to the average partial sensitivity when calculated in this way. This can be achieved by measuring the track densities induced by planar surfaces parallel to the detector that intersect the effective volume.

Since alpha particles emitted by the ^{241}Am source have almost the same energy as those emitted by radon atoms (5.49 MeV), the source surface will intercept the effective volume of radon by moving the source at different distances from detector. As a result, circular effective surfaces are created at the source from which the emitted alpha particles have non-zero probability of inducing visible etched tracks under an optical microscope. The effective surfaces are the cross sections between the effective volume and the planar source at different source-detector distances.

3. Monte Carlo simulations

3.1. Program description

Partial sensitivity of the bare LR-115 detector to radon, thoron or their progenies was calculated by a self-developed computer program based on Monte Carlo simulations. The program performs simulations of alpha particles emitted by a planar ^{241}Am source and their registration by detector. For simulations, starting points of alpha particles are randomly sampled in circles parallel to the detector plane. Distances between circles and detector are varied with a small step. Only alpha particles emitted inside the volume defined by the horizontal cross section of the effective volume are registered by detector.

Inputs of the program.

1. Energy of alpha particles emitted by the source.
2. Database of critical angles as a function of alpha energy (of the energy window) for different detector residual thicknesses.
3. Residual layer thickness.
4. Radii of detector (r_d) and the ^{241}Am source (r_s), and step for the source-detector distances (s).

3.2. Program calculations and steps

3.2.1. Determination of detection efficiency

1. Determination of the energy window [$E_{\min}$, $E_{\max}$] and critical angle as a function of energy [$\theta_c = f(E)$] for given detector residual thickness. This was accomplished by linear interpolation on the database of track parameters obtained with the TRACK_TEST program written by Nikezic et al. (2021). Database was generated by systematically varying the incident alpha particle energy from 0.8 to 4.8 MeV (0.2 MeV steps) and the incident angle from 30° to 90° (5° steps) for etching times from 105 to 125 min (5-min steps). Only simulated tracks that perforate the active layer of the LR-115 detector were considered. The mass etching rate of 3.27 μm h^{-1} corresponding to standard etching conditions was adopted (Nikezic and Janicijevic, 2002). The Durrani-Green's V function with constants $a_1 = 14.50$, $a_2 = 0.50$, $a_3 = 3.9$, $a_4 = 0.066$ and $a_5 = 1$ was used (Durrani and Green, 1984). Fig. 1A shows the results of critical angles as a function of energies for different detector residual thicknesses. From this graph, energy windows for different residual thicknesses of detector active layer can be determined considering that for $E_{\min}$ and $E_{\max}$ the critical angles are the same (90°). The V function used in this work adequately described the experimental results obtained by Leung et al. (2007) and Nikezic and Yu (2010). Furthermore, the energy window and average critical angle obtained using that function were close to those obtained experimentally by Rojas et al. (2018) (the percentage difference between theoretical and experimental parameters did not exceed 5%).
2. Calculation of the minimum [$d_{\min} = R_0 - R$ ($E_{\max}$)] and maximum [$d_{\max} = R_0 - R$ ($E_{\min}$)] distances travelled by alpha particles so that their energies fall within the energy window (Fig. 1B). Alpha particle ranges (R_0) and energy losses in air were obtained from data provided by the SRIM-2013 program. Fig. 1B also shows the longitudinal section of the effective volume, considering constant critical angle, and its intersections with several horizontal planes. Experimentally, this can be achieved by consecutively exposing LR-115 detectors at different distances from a planar alpha source. Requirements to be met by the source are two: the alpha particle emission energy must be larger than $E_{\max}$ of the energy window, and its radius must be greater than the radius of the largest circle that can be created by the

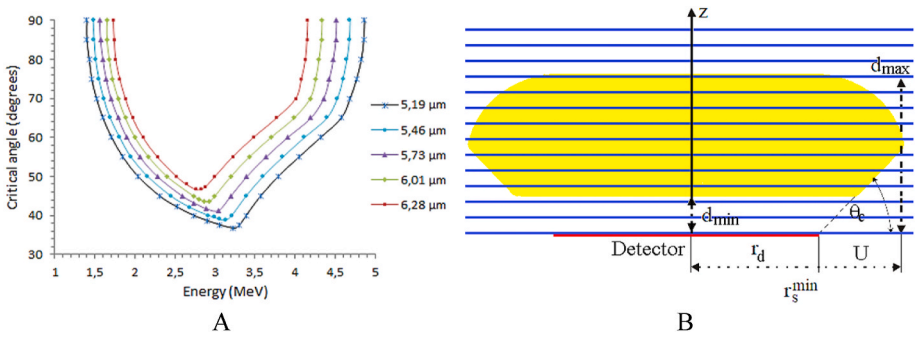

Fig. 1. A. Data set of $\theta_c = f(E)$ obtained for different residual layer thickness of detector active layer. B. Longitudinal section of the effective volume considering the average critical angle (yellow shading) for an LR-115 detector. Blue lines represent planar surfaces parallel to detector plane intersecting the effective volume.

intersection of horizontal planes with the effective volume (r_s^{min} in Fig. 1B).

3.Sampling of N random starting points of alpha particles on a circular surface of radius r_s located at different distances from the detector, simulating the emission of alpha particles from the planar source. Only alpha particles emitted from effective surfaces can be registered in detector.

4. Sampling of random direction of alpha particle emission.
5. Evaluation of alpha particle interaction with detector. If alpha particle does not hit the detector, a new particle is generated and steps from number 3 are repeated.
6. Detection of the incident alpha particle is evaluated by compliance or not with the energy and angle restrictions. If "yes", the counter (N_d) of registered alpha particles is increased by 1. If "no", a new particle is generated and steps from number 3 are repeated.

Once a theoretical value for the distance between the alpha source and the detector is set, uniformly distributed random positions are simulated on the surface of the alpha source. Isotropic emissions of alpha particles are then simulated from each created position. For directions that intersect with the detector, distances between the emission point and the point of intersection with the detector, as well as the incident angle, are calculated. These are the distances travelled by alpha particles in ambient air, whose density depends on pressure, temperature, and humidity. Alpha particles that impact the detector will have travelled different distances in the air, so they arrive with energies and angles within a wide range depending on thickness of the air layer present between the source and detector. Impact energies were estimated from the stopping power vs. energy data provided by the SRIM-2013 program, where the air density has been corrected according to ambient conditions. By considering the real air density in the simulated experiments, it is expected that they will be consistent with experimental results.

Steps 3–6 are repeated until the desired track density is reached. Detection efficiency is then calculated as the ratio between the number of registered (N_d) and emitted alpha particles (N) ($\varepsilon = N_d/N$). The number of tracks detected for each source-detector distance is accumulated in a counter c:

$$c = \sum_{i=1}^{n} N_{d_i}, \tag{2}$$

where n is the number of generated planar surfaces that conditioned the formation of visible tracks in detectors; it depends on the step length.

3.2.2. Determination of partial sensitivity

The cumulative or intrinsic efficiency is the fraction of the number of alphas registered by the detector ($\sum_{i=1}^{n} N_{d_i}$) out of the total alpha particles (nN) emitted within the volume of a cylinder of radius r_s and height given by the difference (d_{max} - d_{min}):

$$\varepsilon_c = \frac{\sum_{i=1}^{n} N_{d_i}}{nN} = \frac{1}{n}\sum_{i=1}^{n} \varepsilon_i = \langle \varepsilon \rangle, \tag{3}$$

In other words, the cumulative efficiency can be calculated as the average of detection efficiencies obtained for the different source-to-detector distances.

The average concentration of the species (C), track density (T), exposure time (t) and partial sensitivity (K_B) are related by the following formula:

$$K_B = \frac{T(tracks.m^{-2})}{C(Bq.m^{-3})t(s)} \tag{4}$$

The total number of particles emitted per 1 s in the volume above the detector in the interval of distances where alpha particles are detected, (d_{max} - d_{min}), can be expressed as VCt [with $V = \pi r_s^2(d_{max} - d_{min})$]. Multiplying it by the cumulative detection efficiency gives the number of registered tracks. Dividing this by the detector area, the track density can be calculated as:

$$T\left(tracks.m^{-2}\right) = \frac{CVt}{\pi r_d^2}\varepsilon_c, \tag{5}$$

From Eqs. (4) and (5) it follows that simulated partial sensitivity is given by:

$$K_B = \frac{V}{\pi r_d^2}\varepsilon_c = \varepsilon_c(d_{max} - d_{min})\left(\frac{r_s}{r_d}\right)^2 \tag{6}$$

If all detectors have the same area, and are exposed during the same time, the experimental cumulative efficiency can be calculated by:

$$\varepsilon_c = \frac{\pi r_d^2 \sum_{i=1}^{n} T_i}{nAt} = \frac{\pi r_d^2}{At}\langle T \rangle \tag{7}$$

where A is the emission rate (activity in Bq) of the planar alpha source and n is the number of heights between d_{min} and d_{max}, i.e. the number of detectors that registered alpha tracks. Partial sensitivity is then expressed as:

$$K_B = \frac{\pi r_s^2(d_{max} - d_{min})}{At}\langle T \rangle \tag{8}$$

Thus, K_B can be calculated by measuring the track density for each source-to-detector distance, and averaged over all distances, and knowing the range of distances that produce visible tracks in detectors, the source radius and the surface source activity.

In summary, using a planar alpha source of known activity (^{241}Am, ^{244}Cm, ^{210}Po, or any other with E > E_{max}) the partial sensitivity of the bare LR-115 detector to radon, thoron and their alpha-emitting airborne progeny can be determined. It is worth mentioning that the obtained

value of partial sensitivity corresponds to certain energy window and critical angle, both depending on etching conditions and track reading method.

The minimum radius of the alpha source (r_s^{min}) can be estimated from the radius of the largest effective circle which can be approximated as:

$$r_s^{min} = r_d + \{R(E_0) - R[E(\theta_c^{min})]\}\cos\theta_c^{min}, \quad (9)$$

for critical angle as a function of incident alpha particle energy [$\theta_c = f(E)$], where θ_c^{min} is the smallest critical angle, or more roughly as:

$$r_s^{min} = r_d + d_{max}\cos\overline{\theta_c}, \quad (10)$$

for critical angle equal to the average value of the function $\theta_c = f(E)$ ($\overline{\theta_c}$), evaluated in the energy window corresponding to the residual thickness of detector. Summarizing, source size depends on alpha particle emission energy, detector size, and etching conditions.

4. Results of simulations and discussion

Unless other parameters are indicated, the following are used in simulations: A circular ^{241}Am source emitting alpha particles with 5.49 MeV. Nominal activity of the ^{241}Am reference source RRS type 21 A (2446 alpha particles per second) and detector exposure times of 30 min. Although the program is designed for any residual thickness between 5.19 and 6.28 μm, a residual detector thickness of 5.46 μm will be used for which the interpolated energy window is [1.48, 4.69] MeV. The detector radius (r_d) is 0.5 cm and that of the source (r_s) is slightly larger than the minimum value calculated by Eq. (10). Step length of 0.1 cm for the distances between the source and the detector. Data of $\theta_c = f(E)$ corresponding to the assumed residual thickness (Fig. 2); the average critical angle is also used for some calculations.

4.1. Variation of effective surface, track density, and partial sensitivity when varying the source-detector distance

Fig. 2 shows the simulated starting points that generated visible tracks on the LR-115 detector – horizontal lines represent the cross-sections of the planar source, at different positions, and the vertical plane. As can be seen, the emission points delineate the ^{241}Am effective volume and the minimum surface that the source must have in order that all the effective volume of alpha emissions can be simulated. Similar results have been obtained for other alpha particle sources with energies higher or lower than that of ^{241}Am, provided they are greater than E_{max}.

As inferred from Fig. 2, the effective surface increases as the source-detector distance increases from position 1 to 2. Around position 2 it increases sharply and then increases slightly until it reaches its maximum value. From there it begins to decrease monotonically to position 3. This behaviour results from the way in which the radius of the effective circle changes as the source-detector distance increases, as shown in Fig. 3. In that figure it is also possible to identify the maximum alpha energies at which the most important changes in the effective surface occur and also indicate the energy window.

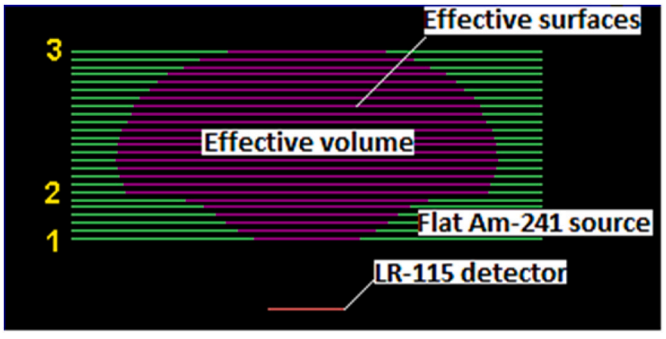

Fig. 2. Simulated starting points on the horizontal cross sections that generated countable tracks on the LR-115 detector. Green and purple lines represent longitudinal sections of the planar source and the effective surfaces (formed by the intersections of the planar source with the effective volume), respectively.

Fig. 4 shows the variation of track density and partial sensitivity as a function of the source-detector distance assuming two cases for the critical angle: $\theta_c = f(E)$ (Fig. 1A) and $\theta_c = \overline{\theta_c} = 52°$. The behaviour of the track density is similar to that of the effective surface due to the proportionality between them. Track density is constant over a wide range of source-detector distance values when $\overline{\theta_c}$ is used. For $\theta_c = f(E)$ the track density increases sharply up to about 1.5 cm, similar to the effective circle radius, and thereafter it rapidly decreases unlike the effective surface radius. The behaviour of curves reflects the energetic and angular constraints dependent on the V function that characterizes the formation of etched tracks. Similar to the track density, K_B equals zero at short distances and then increases with increasing distance to detector until it reaches a maximum. From there, K_B values for the two cases of θ_c get closer and become equal at the largest distance in which track density is different from the background (0.2225 ± 0.0007) cm. The equality of partial sensitivities, regardless of the assumed model for critical angle, is important from a practical point of view since calculations are much easier and faster assuming constant critical angle.

4.2. Dependence on the energy of alpha particles emitted by the source

To demonstrate that the partial sensitivity obtained by applying the proposed method reflects the physical aspect of partial sensitivity constancy, regardless of the species, and that its value is consistent with results obtained by other methods, virtual planar sources with different alpha emission energies were simulated. As the alpha emission energy must be larger than the maximum energy window, isotopic sources of ^{241}Am, ^{244}Cm, and ^{210}Po were used in simulations. Table 1 shows the partial sensitivities of the LR-115 detector to the mentioned isotopic sources, and to sources emitting alpha particles with energy equal to that of ^{222}Rn, ^{220}Rn, and their short-lived progeny.

The last row of Table 1 shows the percentage variation of K_B values using the partial sensitivity of ^{222}Rn as a reference. As can be seen, the values of partial sensitivities are very close to each other; the maximum percentage variation is around 1%. Equality in partial sensitivities indicates that the developed program adequately describes the nature of physical processes involved in the response of the bare LR-115 detector.

4.3. Relationship with the closed mode of exposure

The information presented thus far pertains to the bare exposure

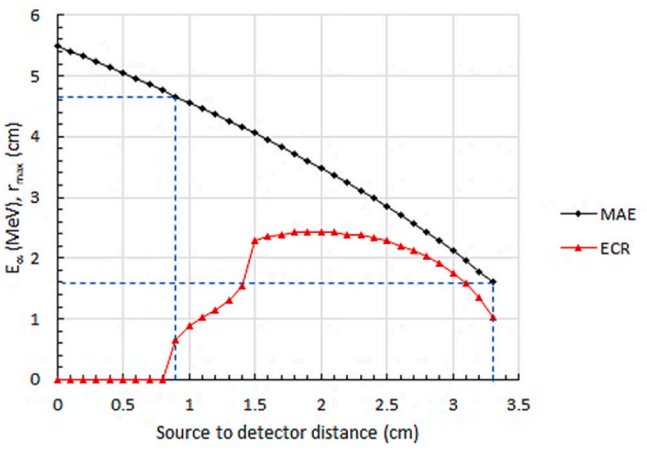

Fig. 3. Maximum alpha particle energy (MAE) and effective circle radius in the ^{241}Am planar source (ECR) for different source-to-detector distances.

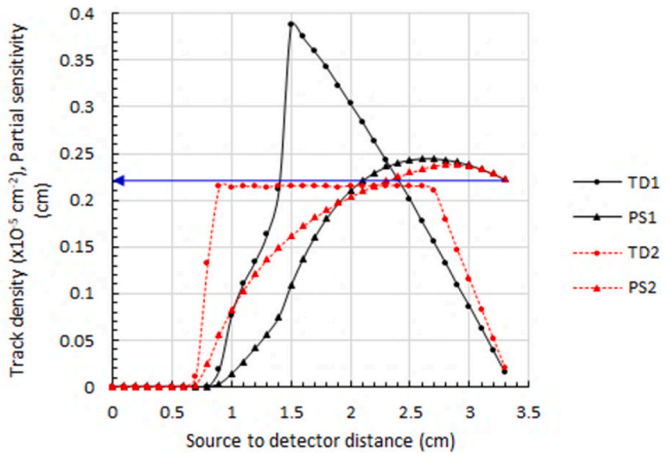

Fig. 4. Dependence of the track density and partial sensitivity of the bare LR-115 detector with the source-to-detector distance for $\theta_c = f(E)$ (TD1 and PS1, respectively) and $\theta_c = \overline{\theta_c} = 52^\circ$ (TD2 and PS2, respectively).

mode of the LR-115 detector. However, it may be of interest to analyse how the situation changes when the detector is used in a closed mode, such as in a diffusion chamber, cup, or similar device.

There exist significant differences between the bare and closed exposure modes. In the former case, the detector records alpha particles emitted by radon, thoron, and their non-equilibrated progeny from their respective effective volumes. In contrast, in a diffusion chamber that discriminates against thoron entry, the detector records alpha particles from radon and its equilibrated progeny, the latter distributed throughout the chamber's volume and/or deposited on its internal and detector surfaces.

Using the CR-39 detector, Askari et al. (2008) demonstrated that in cylindrical diffusion chambers with a radius and height greater than critical values (R_c and h_c, respectively), alpha particles emitted from internal surfaces of the chamber cannot reach the detector as they are stopped by air between the emission position and detector. For such cases, the partial sensitivities of the CR-39 detector remain constant but differ for each alpha emitter.

A similar situation arises for cylindrical chambers with LR-115 detectors inside, but in this case, the partial sensitivities are the same for all species. The values of R_c and h_c can be estimated by considering the energy and angle restrictions for the registration of alpha particles. For an alpha particle-emitting species with energy E_0, R_c is equivalent to the minimum radius of the planar alpha source $r_s^{\min}$, which can be estimated from equation (9) or (10), and h_c is the maximum distance an alpha particle can travel in air to be registered in the detector ($d_{\max}$). Thus, for a diffusion chamber with a radius and height larger than $r_s^{\min}$ and $d_{\max}$, respectively, corresponding to the most energetic alpha-emitting specie, the detector behaves as if it were exposed in bare mode. As a result, partial sensitivities of all airborne species are the same and equal to K_B. Summarizing, the partial sensitivity of the LR-115 detector in closed mode to an airborne species is equal to that of the bare mode if the effective volume of the species does not intersect any internal surface of the diffusion chamber.

The critical values of R_c for radon isotopes and their progeny (shown in Table 1 as $r_s^{\min}$) allow us to infer that an LR-115 detector with a radius of 0.5 cm behaves like a bare detector if the radius and height of the diffusion chamber are larger than 6 cm and 8 cm, respectively. The value of 8 cm is an approximate value of $d_{\max}$ for alpha particles emitted by ^{212}Po, as shown by Mitev et al. (2020).

4.4. Dependence on detector and source radii

The possible influence of source and detector sizes on simulated values of partial sensitivity and track density at the largest source-to-detector distance (minimum track density) was evaluated. For this purpose, combinations of detectors and sources with different radii were used. For detectors with radii of 0.5 cm, 1 cm and 2 cm the respective minimum radii of the source are 2.35 cm, 2.85 cm and 3.85 cm [according to Eq. (9)]. Results shown in Table 2 indicate the weak influence of detector and source dimensions on the calculated values of partial sensitivities in a wide range of combinations.

As in Table 1, Table 2 shows that all partial sensitivities have the same value of 0.22 cm if rounded to two decimal places. As expected, the minimum track density will be lower the larger the source area. However, that track density does not depend on detector size for a given size of the source. $\overline{K_B}$ corresponds to the average of five runs and σ is the standard deviation for each measurement set. The comparison of partial sensitivities with the obtained for $r_d = 1$ cm and $r_s = 3$ cm is presented in the last row of Table 2. For these radii the sampled volume (volume of emission of alpha particles) is very close to the effective volume; under these conditions the calculated sensitivity would be closer to the real value for the considered step. Results indicate independence of the partial sensitivity value with the size of the source and detector as long as the mentioned conditions are met.

4.5. Step length dependence and comparison with partial sensitivities reported by other authors

Table 3 shows the results obtained by varying the step length in simulations. "Total Time" refers to the time required to cover all measurements. The limits of the effective volume in the z-axis are practically covered by the smallest step (0.1 cm). The small difference in sensitivities is because some fraction of the effective volume can be lost depending on the step size as shown in Fig. 1.

As can be seen in Table 3, a good estimate of K_B can be achieved using 5 or 9 detectors in the range of source-detector distances that produce visible tracks for step lengths of 0.5 cm or 0.3 cm, respectively. In that case, total measurement time could be less than 5 h. The maximum percentage deviation of partial sensitivities relative to the K_B value calculated for the smallest step is approximately 10%. Since values of $d_{\min}$ and $d_{\max}$ are not known in advance, total times will be somewhat larger than the estimated times. Nevertheless, they will be relatively small compared with that used for detector calibration in radon chambers. Obviously, the exposure time of detectors can be further reduced if a source with higher activity is used.

Table 3 also shows that if partial sensitivities expressed in cm are rounded to one decimal place and those expressed in tracks. cm-2 per Bq.d.m-3 are rounded to two decimal places, then all values converge to

Table 1
Calculated partial sensitivities of an LR-115 detector to three alpha isotopic sources and to radon, thoron and their progenies.

Source	^{244}Cm	^{210}Po	^{222}Rn	^{218}Po	^{214}Po	^{220}Rn	^{216}Po	^{212}Bi	^{212}Po
α-energy (MeV)	5.80	5.30	5.49	6.00	7.69	6.29	6.78	6.07	8.78
$r_s^{\min}$ (cm)	2.63	2.18	2.35	2.81	4.59	3.10	3.59	2.88	5.92
r_s (cm)	2.7	2.3	2.5	2.9	4.7	3.2	3.7	3.0	6.0
K_B (cm)	0.2154	0.2158	0.2154	0.2157	0.2172	0.2170	0.2182	0.2169	0.2183
PV (%)[a]	0	0.2	0	0.1	0.8	0.7	1.3	0.7	1.3

[a] Percentage Variation.

Table 2
Detector response to different combinations of source and detector radii (r_s and r_d, respectively). The partial sensitivities presented are mean values of 5 runs of the program, with the standard deviations (σ) shown. In the last row are the deviations of each sensitivity to the value obtained for $r_d = 1$ cm and $r_s = 3$ cm.

r_s (cm)	3			5			7		
r_d (cm)	0.5	1	2[a]	0.5	1	2	0.5	1	2
Minimum track density (tracks.cm^{-2})	1052	1077	–	378	380	386	197	186	194
$\overline{K_i}$ (cm)	0.2161	0.2155	–	0.2163	0.2162	0.2159	0.2202	0.2156	0.2158
σ (cm)	0.0002	<0.0001	–	0.0002	<0.0001	0.0001	0.0001	0.0001	0.0001
Deviations (%)	0.30	0.00	–	0.38	0.34	0.17	2.16	0.05	0.17

[a] The minimum source radius is larger than 3 cm for this detector radius.

Table 3
Detector response in dependence on the step length for the source-to-detector distances.

Step (cm)	Total time (h)	Num-ber of detec-tors	d_{min} (cm)	E_{max} (MeV)	d_{max} (cm)	E_{min} (MeV)	$r_d = 0.5$, $r_s = 4$	$r_d = 1$, $r_s = 4$	$r_d = 1$, $r_s = 3$	K_B (tracks.cm^{-2} per Bq.d.m^{-3})
							K_B (cm)	K_B (cm)	K_B (cm)	
0.05	25	50	0.9	4.66	3.35	1.5	0.22	0.22	0.22	0.019
0.1	12.5	25	0.9	4.66	3.3	1.59	0.22	0.22	0.22	0.019
0.2	6	12	1.0	4.56	3.2	1.77	0.20	0.20	0.20	0.017
0.3	4.5	9	0.9	4.66	3.3	1.59	0.21	0.21	0.21	0.018
0.5	2.5	5	1.0	4.56	3	2.1	0.20	0.20	0.20	0.017

0.2 cm and 0.02 tracks. cm-2 per Bq.d.m-3, respectively, which are similar to those obtained by Leung et al. (2006) in the HPA walk-in exposure chamber. Our value is also comparable with the theoretical and experimental mean value (0.23 cm <> 0.02 tr. cm^{-2}/Bq.d.m^{-3}) reported by Eappen and Mayya (2004). The slight disagreement may be due to small differences between the etching conditions and reading mode used by these authors and those assumed in this work. It is worth noting that theoretical approaches used by these authors were different from those used in this work. Higher sensitivity values have been reported (Planinic, 1992); in that case the visibility criterion did not imply total detector perforation and correction of the critical angle was not considered for pronounced impact angles.

Table 4 presents a comparison of the average partial sensitivity value obtained in this work with partial sensitivity values reported by other authors. The percentage difference between the KB estimated using our method and that reported by other authors is expressed by the percentage difference, Diff (%), which was calculated as

Table 4
Comparison of the average partial sensitivity obtained in this work with the theoretically and experimentally reported by other authors.

Partial sensitivity (tr.cm^{-2}/Bq.d.m^{-3})	Mode	Authors	Observations	Diff (%)
0.021 ± 0.003	Experimental	Mayya et al. (1998)	Equilibrium factors Radon- [~0–0.8] Thoron [~0–0.15]	8.6
0.023	Experimental	Faj and Planinic (1991)	ΔE = [1.7, 4.1] MeV $\overline{\theta_c} = 40°$	16.5
0.022	Theoretical			12.7
0.02	Theoretical	Eappen and Mayya (2004)	–	4.0
0.0200 ± 0.0017	Experimental		For radon	4.0
0.0196 ± 0.0015	Experimental		For thoron	2.0
0.0203	Experimental	Leung et al. (2006)	Residual active layer thickness- 5.46 μm	5.5
0.0249	Theoretical	Yu et al. (2005)	Residual active layer thickness- 5.46 μm	22.9
0.0197	Theoretical	Rojas et al. (2018)	ΔE = [1.48, 4.69] MeV, $\overline{\theta_c} = 53°$	2.5
0.0192 ± 0.0001	Theoretical	This work	Residual active layer thickness- 5.46 μm	–

$$Diff(\%) = \left|\frac{K_B^i - K_B^{TW}}{K_B^i}\right| x100 \quad (11)$$

where K_B^i and K_B^{TW} are the sensitivities reported in other studies and in this study, respectively.

As can be seen in Tables 4 and in most cases the percentage difference was less than 20%, even though in some of them the etching conditions, track reading mode, track formation model, or experimental method used differed to some extent from those assumed in this work, suggesting that our method exhibits good performance and has the advantage of being simple, easy to implement, cost-effective, and fast. The largest difference between the theoretical results of this work and that of Yu et al. (2005) may be attributed to the use of different V functions.

4.6. Influence of the active layer thickness of alpha sources on sensitivity calculations

It could be supposed that previously obtained results are only valid for ideal sources (with negligible thickness). However, since the LR-115 detector response depends mainly on the difference between the maximum and minimum allowed distances, the partial sensitivity might not be affected by the use of relatively thick sources. In planar sources constructed from anodized aluminium foils the activity is incorporated in the top surface of an aluminium foil resulting in a source which has an active layer of about 5 μm (0.8 mg cm^{-2}) in depth. The developed program was slightly modified to consider a finite thickness of the alpha source where the ^{241}Am atoms are uniformly distributed. Energy of the alpha particle emerging from the source is calculated from the energy-distance curve obtained by SRIM2013 using a material with density and composition very close to that of the active source material. Through Monte Carlo simulations the energy distributions of alpha particles emerging from the surface of the ^{241}Am source were determined. The frequency histograms for two different thicknesses of the active layer are shown in Fig. 5. In both cases the number of generated histories was the same.

At greater thickness of the active layer the number of alpha particles with energies above E_{max} decreases and the number of particles with energies comprised within the energy window increases. Consequently, the probability of registration of alpha particles emitted at lower source-detector distance grows and particles can even be registered at zero

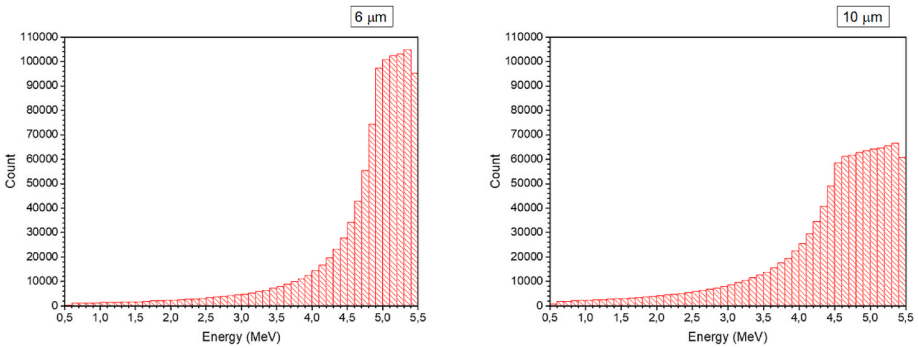

Fig. 5. Energy distribution of alpha particles emerging from planar ^{241}Am sources having active layer thicknesses of 6 µm (left) and 10 µm (right).

distance. Fig. 6 shows the cross-section of the intersections of alpha-emitting planar surfaces with the effective volume for an ideal source and for sources with active layers of different thicknesses. The input data for simulations were $r_d = 0.5$ cm, $r_s = 4$ cm, $s = 0.1$ cm, energy window [1.48, 4.69] MeV and $\theta_c = f(E)$ from Fig. 2.

Results of simulations show that partial sensitivities are practically the same; the percentage differences regarding the sensitivity of the ideal source are about 1%. However, the shapes, dimensions and locations of effective volumes are different. With increased thickness of the active layer the effective volume becomes larger and visible tracks are induced in detector at a smaller distance from the source. For example, to induce visible tracks on an LR-115 detector facing an ideal planar source the distance between them cannot be less than 0.9 cm (for the step used in simulations). However, visible tracks are produced at 0 cm source-to-detector distance for a 10 µm active-thickness source. Although there is a slight increase in partial sensitivity up to a 10 µm thick active layer, it is expected to decrease for larger thicknesses due to alpha particle self-absorption. For the above reasons, the nature of active material must be known in order to have an idea of the minimum source-detector distance at which tracks begin to be registered.

4.7. Influence of thoron and its progeny on radon measurements

When the bare mode is applied in radon measurements, ^{220}Rn atoms and their alpha-emitting progeny present in air will contribute tracks on the LR-115 detector, leading to erroneous estimations of radon concentrations. Corrections must be performed to account for the number of interfering tracks.

The track density registered on a detector exposed to a mixed environment containing radon, thoron, and their progeny, ρ_B^{ME}, can be expressed as (Mayya et al., 1998; Ramachandran et al., 2003):

$$\rho_B^{ME} = K_B t\left[C_{^{222}Rn}\left(1+F_p\right) + C_{^{220}Rn}\left(2+f_4^{'}\right)\right] \tag{12}$$

where $F_p = \frac{C_{^{218}Po}}{C_{^{222}Rn}} + \frac{C_{^{214}Po}}{C_{^{222}Rn}}$ (proxy equilibrium factor) and $f_4^{'} = \frac{C_{^{212}Po}}{C_{^{220}Rn}}$.

If the concentration of thoron and its progeny can be neglected, the track density registered on the detector during the same time t would be given only by the contributions of radon and its non-equilibrated progeny (Yu et al., 2008; Choi et al., 2010; Yu and Nikezic, 2011):

$$\rho_B^{Rn} = C_{^{222}Rn} K_B t\left(1+F_p\right) = S_B^{Rn} C_{^{222}Rn} t \tag{13}$$

where S_B^{Rn} is the calibration factor of the bare detector that relates the track density rate to the radon concentration and can be experimentally determined in a radon chamber under similar environmental conditions as those of detector exposure.

The correction of the track density registered in the bare LR-115 detector, i.e., the removal of the influence of thoron and its progeny on the track density due to radon, can be achieved by subtracting equation (13) from equation (12) and considering the approximation

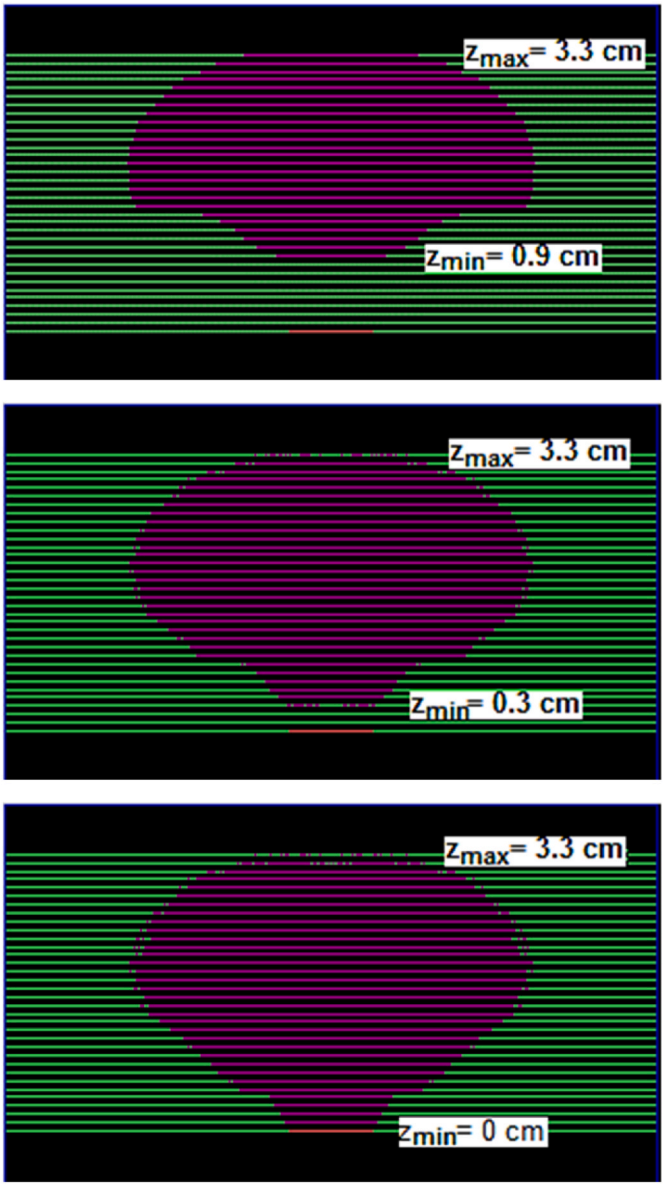

Fig. 6. Cross sections of effective volumes for ^{241}Am sources with active thicknesses of 0 µm (A), 6 µm (B) and 10 µm (C). Partial sensitivities calculated by Monte Carlo simulations were 0.2169 cm, 0.2185 cm and 0.2196 cm, respectively. Red line below the effective volume represents the LR-115 detector.

suggested by Choi et al. (2010) for practical purposes of correction under normal situations:

$$\Delta\rho = \rho_B^{ME} - \rho_B^{Rn} = 2C_{^{220}Rn}K_B t \tag{14}$$

Equation (14) shows that the presence of thoron affects the track density in the detector and in turn gives the correction to be made. The track density corresponding to radon and its progeny corrected by the contribution of thoron can be estimated as:

$$\rho_B^{Rn} = \rho_B^{ME} - 2C_{^{220}Rn}K_B t \tag{15}$$

where the value of K_B estimated according to the method presented in this work would be applied. Considering equation (13), the radon concentration in a mixed environment can be estimated as:

$$C_{^{222}Rn} = \frac{\rho_B^{ME}}{S_B^{Rn} t} - 2\frac{K_B}{S_B^{Rn}}C_{^{220}Rn} \tag{16}$$

The first term of equation (16) represents the uncorrected radon concentration, overestimated due to the presence of thoron. Clearly, if thoron concentration can be neglected, the actual radon concentration could be measured using only that term.

Results presented in this work may be applicable on thoron measurements. If radon concentration $C_{^{222}Rn}$ is determined, for example, with a thoron-discriminating diffusion chamber, thoron concentration can be estimated from equation (16) as:

$$C_{^{220}Rn} = \frac{1}{2}\left(\frac{\rho_B^{ME}}{S_B^{Rn} t} - \frac{S_B^{Rn}}{K_B}C_{^{222}Rn}\right) \tag{17}$$

Due to uncertainties in experimental measurements, equations (16) and (17) may generate negative values.

In regard to the thoron progeny, although considering the bifurcation of ^{212}Bi is not relevant for the calculation of partial sensitivity (see Table 1), a correction factor for the alpha emission percentage is necessary when calculating, for instance, the contribution of airborne ^{212}Bi or ^{212}Po to the track density.

Without considering the issue of the large spatial disequilibrium between thoron and its progeny, where ^{220}Rn shows a non-homogeneous distribution due to its short half-life unlike its progeny, according to equation (12) the track density contributed by thoron and its airborne progeny in the bare LR-115 detector can be expressed as:

$$\rho_B^{^{220}Rn} = K_B C_{^{220}Rn} t\left(2 + f_4^{'}\right) \tag{18}$$

Equation (18) results from considering that ^{216}Po and ^{212}Po practically decay upon formation due to their very short half-lives, so that the former will always be in equilibrium with ^{220}Rn while the latter will be in equilibrium with ^{212}Bi. ^{212}Bi undergoes double splitting with 36% decay by emission of alpha particles of 6.05 MeV, while the remaining fraction (64%) decays almost instantaneously by beta emission into ^{212}Po which in turn decays emitting alpha particles of 8.78 MeV. That is, equation (18) arises from the following expression:

$$\rho_B^{^{220}Rn} = K_B t\left(C_{^{220}Rn} + C_{^{216}Po} + 0.36C_{^{212}Bi} + 0.64C_{^{212}Bi\left(^{212}Po\right)}\right) \tag{19}$$

Thus, the individual contributions of airborne ^{212}Bi and ^{212}Po to the track density must include the correction factors for the alpha emission percentage of each radionuclide as:

$$\rho_B^{^{212}Bi} = 0.36K_B C_{^{212}Bi} t, \text{ and } \rho_B^{^{212}Po} = 0.64K_B C_{^{212}Po} t \tag{20}$$

Finally, we would like to highlight that the contribution of radon/thoron and their progeny in the surrounding environment to the registered track density, as well as the reduction of progeny concentration near the detector due to the plate-out effect, were assumed to be negligible and were not considered in simulations. This can be justified by considering that detectors are typically exposed for a relatively short period of time in practice, and laboratory environments generally have low levels of radon/thoron resulting in low background track densities. Furthermore, the use of a high-activity alpha source ensures that almost all the tracks registered in detector originate from alpha particles emitted by the ^{241}Am planar source, which are of interest for calculating partial sensitivities. Hence, we believe that our simulation results accurately represent the sensitivity of the LR-115 detector for alpha particle detection. The low detection of alpha particles generated in the surrounding environment improves the accuracy of results and reduces uncertainties. We would like to emphasize that our simulations were carried out using a large number of histories (approximately 5×10^6) and each experiment was repeated at least three times, resulting in percentage standard deviations of less than 1% in all cases. We are confident that this method yields accurate and precise results.

5. Conclusions

The bases of a method and a simulation program were developed to calculate the partial sensitivity of a bare LR-115 detector to radon, thoron, or any of their progenies, for residual detector thicknesses in the range of 5.19 μm–6.28 μm. Simulation results demonstrated that partial sensitivity can be estimated experimentally by measuring the induced track densities in small detectors exposed at different distances from a planar alpha source. The method, evaluated by simulation experiments, is simpler and faster, compared to the method that uses standard sources of radon and its progeny and a large chamber with controlled conditions. The average value of calculated partial sensitivity is comparable with those obtained theoretically and experimentally by other authors. In addition to electrodeposited sources, relatively thick sources such as those encapsulated with very thin metal foil or constructed from anodized aluminium foil can be used. The consistency of the partial sensitivity value to variations in the source and detector sizes, the alpha particle emission energy, the step length for source-detector distances, and the thickness of the source active layer was demonstrated. Given the ease of calibration and use, low cost and versatility, the LR-115 detectors continue to be a good alternative for measurements of radon isotopes and their progeny, so it is suggested to continue using them.

Declaration of competing interest

The authors declare that they have no known competing financial interests or personal relationships that could have appeared to influence the work reported in this paper.

Data availability

Data will be made available on request.

Acknowledges

This study has been partially financed by the Brazilian Agency FAPESP (N 2013/13238–5) and by the Annual Research Project supported by PUCP (CAP 2021-A-0024/PI0736).

References

Abo-Elmagd, M., Mansy, M., Eissa, H.M., El-Fiki, M.A., 2006. Major parameters affecting the calculation of equilibrium factor using SSNTD-measured track densities. Radiat. Meas. 41 (2), 235–240.

Askari, H.R., Ghandi, K., Rahimi, M., Negarestani, A., 2008. Theoretical calculation on CR-39 response for radon measurements and optimum diffusion chambers dimensions. Nucl. Instrum. Methods Phys. Res. B 596 (3), 368–383.

Baggs, S.A., Wong, C.F., 1987. Survey of radon in Australian residences. Architect. Sci. Rev. 30 (1), 11–21.

Banjanac, R., Dragić, A., Grabez, B., Joković, D., Markushev, D., Panic, B., Udovičić, V., Anicin, I., 2006. Indoor radon measurements by nuclear track detectors: applications in secondary schools. FU Phys. Chem. Tech. 4 (1), 93–100.

Choi, V.W., Ng, C.K., Lam, R.K., Janik, M., Sorimachi, A., Kranrod, C., et al., 2010. Long-term determination of airborne radon progeny concentrations using LR 115 detectors and the effects of thoron. Radiat. Protect. Dosim. 141 (4), 404–407.

Durrani, S.A., Green, P.F., 1984. The effect of etching conditions on the response of LR 115. Nucl. Tracks 8, 21–24.
Eappen, K.P., Mayya, Y.S., 2004. Calibration factors for LR-115 (type-II) based radon thoron discriminating dosimeter. Radiat. Meas. 38, 5–17.
Faj, Z., Planinic, J., 1991. Dosimetry of radon and its daughters by two SSNT detectors. Radiat. Protect. Dosim. 35, 265–268.
Kitson-Mills, D., Sovoe, S., Opoku-Ntim, I., Adesi, K., Marnotey, S., Anim-Sampong, S., Addo, M., Otoo, F., Baiden, F., 2019. An assessment of indoor radon level in a suburb of Ghana. Environ. Res. Commun. 1, 061002.
Leung, S.Y.Y., Nikezic, D., Yu, K.N., 2006. Passive monitoring of the equilibrium factor inside a radon exposure chamber using bare LR 115 SSNTDs. Nucl. Instrum. Methods Phys. Res. A. 564, 319–323.
Leung, S.Y.Y., Nikezic, D., Yu, K.N., 2007. Derivation of V function for LR 115 SSNTD from its partial sensitivity to 222Rn and its short-lived progeny. J. Environ. Radioact. 92, 55–61.
Loffredo, F., Opoku-Ntim, I., Kitson-Mills, D., Quarto, M., 2022. Gini method application: indoor radon survey in kpong, Ghana. Atmosphere 13, 1179.
Mayya, Y.S., Eappen, K.P., Nambi, K.S.V., 1998. Methodology for mixed field inhalation dosimetry in monazite areas using a twin-cup dosemeter with three track detectors. Radiat. Protect. Dosim. 77 (3), 177–184.
Miles, J.C., Stares, E.J., Cliff, K.D., Sinnaeve, J., 1984. Results from an international intercomparison of techniques for measuring radon and radon decay products. Radiat. Protect. Dosim. 7 (1–4), 169–173.
Miller, C.A., Howarth, C.B., 2022. Results of the 2021 Intercomparison of Passive Radon Detectors. UK Health Security Agency RCE-002.
Mitev, K., Cassette, P., Pressyanov, D., Georgiev, S., Dutsov, C., Michielsen, N., Sabot, B., 2020. Methods for the experimental study of 220Rn homogeneity in calibration chambers. Appl. Radiat. Isot. 165, 109259.
Nader, A.F., 2019. The determination of equilibrium factor of radon and thoron using LR-115 type II detector in a selected area from Basra Governorate. Iraq J. Phys. Conf. Ser. 1258, 012032.
Nikezic, D., Janicijevic, A., 2002. Bulk etching rate of LR 115 detector. Appl. Radiat. Isot. 57, 275–278.
Nikezic, D., Yu, K.N., 2007. Computer simulation of radon measurements with nuclear track detectors. In: Bianco, S.J. (Ed.), Computer Physics Research Trends 3. Nova Science Publishers Inc., pp. 119–150
Nikezic, D., Yu, K.N., 2010. Long-term determination of airborne concentrations of unattached and attached radon progeny using stacked LR 115 detector with multi-step etching. Nucl. Instrum. Methods Phys. Res. A. 613 (2), 245–250.
Nikezic, D., Stajic, J.M., Yu, K.N., 2021. Updates to TRACK_TEST and TRACK_VISION computer programs. Polymers 13 (4), 560.
Planinic, J., 1992. The efficiency and angular sensitivity of the LR-115 nuclear track detector to alpha particles. Nucl. Instrum. Methods Phys. Res. B. 71, 95–98.
Pressyanov, D., 2022. New generation of highly sensitive radon detectors based on activated carbon with compensated temperature dependence. Sci. Rep. 12, 8479.
Ramachandran, T.V., Eappen, K.P., Nair, R.N., Mayya, Y.S., Sadasivan, S., 2003. Radon-thoron Levels and Inhalation Dose Distribution Patterns in India Dwellings (No. BARC–2003/E/026). Bhabha Atomic Research Centre.
Rojas, J., Palacios, D., Pereyra, P., Pérez, B., Bohus, L.S., López, M.E., 2018. A semi-empirical approach to estimate the parameters determining the LR-115 detector response in radon measurements. Radiat. Meas. 118, 36–42.
Stevanovic, N., Markovic, V.M., Milosevic, M., Djurdjevic, A., Stajic, J.M., Milenkovic, B., Nikezic, D., 2022. Correlations between track parameters in a solid-state nuclear track detector and its diffraction pattern. Radiat. Phys. Chem. 193, 109986.
Yu, K.N., Nikezic, D., 2011. Long-term determination of airborne radon progeny concentrations using LR 115 solid-state nuclear track detectors. Radiat. Meas. 46, 1799, 476 1802.
Yu, K.N., Nikezic, D., Ng, F.M.F., Leung, J.K.C., 2005. Long-term measurements of radon progeny concentrations with solid state nuclear track detectors. Radiat. Meas. 40, 560, 479.
Yu, K.N., Leung, S.Y., Nikezic, D., Leung, J.K., 2008. Equilibrium factor determination using SSNTDs. Radiat. Meas. 43, S357–S363.
Ziegler, J.F., 2013. SRIM Code V available at. http://www.srim.org/.